High-temperature structural evolution of RNiO$_3$ (R=Ho, Y, Er, Lu) perovskites: Charge disproportionation and electronic localization

J. A. Alonso,* M. J. Martínez-Lope, and M. T. Casais
Instituto de Ciencia de Materiales de Madrid, Consejo Superior de Investigaciones Científicas, Cantoblanco, E-28049 Madrid, Spain

J. L. García-Muñoz
Institut de Ciència de Materials de Barcelona, Consejo Superior de Investigaciones Científicas, Campus UAB, E-08193, Bellaterra, Barcelona, Spain

M. T. Fernández-Díaz
Institut Laue-Langevin, Bôite Postale 156, F-38042 Grenoble Cedex 9, France

M. A. G. Aranda
Departamento de Química Inorgánica, Cristalografía y Mineralogía, Facultad de Ciencias, Universidad de Málaga, E-29071 Málaga, Spain

(Received 31 October 2000; revised manuscript received 7 March 2001; published 31 July 2001)

The structural changes of polycrystalline RNiO$_3$ perovskites (R=Ho, Y, Er, and Lu, prepared under high-oxygen pressure) across the metal-insulator (MI) transition (T_{MI} ranging between 573 and 600 K) have been studied by high-resolution neutron- and synchrotron diffraction techniques. In the insulating (semiconducting) regime, below T_{MI}, the perovskites are monoclinic, space group $P2_1/n$, and contain two chemically different Ni1 and Ni2 cations, as a result of the charge disproportionation (CHD) of Ni^{3+} cations. Above T_{MI} the samples become orthorhombic, space group *Pbnm*. Upon heating across T_{MI}, the CHD vanishes and there is an abrupt convergence of the two sets (Ni1 and Ni2) of three Ni-O bond lengths, in the monoclinic-insulating phase, to three unique Ni-O distances in the orthorhombic-metallic phase. An unexpected expansion of the *b* unit-cell parameter is observed across the electronic transition. This effect, not reported for the former members of the series, is the consequence of an extremely anisotropic rearrangement of Ni-O bonds across the transition. The distortion of the NiO_6 octahedra reaches its maximum value at temperatures close to T_{MI}. The evolution of the mean ⟨Ni-O⟩ bond lengths suggests a gradual increase of the degree of CHD (i.e., the difference between the average size of $Ni1O_6$ and $Ni2O_6$ octahedra) on increasing temperature in the insulating regime, to reach a maximum at 60–80 K below the MI transition.

DOI: 10.1103/PhysRevB.64.094102 PACS number(s): 71.30.+h, 71.45.Lr, 71.38.−k, 75.25.+z

I. INTRODUCTION

The family of RNiO$_3$ perovskites (R=rare-earth metals) offers an excellent opportunity to study a metal-to-insulator (MI) transition in narrow σ^*-band oxides, in which the bandwidth can be significantly varied as the e_g(Ni)-$2p\sigma$(O) covalent mixing is progressively reduced from R=La to Lu. The metallic character of rhombohedral $LaNiO_3$ was reported in 1965 (Ref. 1); it exhibits Stoner enhanced Pauli paramagnetism by the proximity to the critical bandwidth.[2,3] Along the RNiO$_3$ family, the susceptibility evolves from Pauli to Curie-Weiss paramagnetism with decreasing bandwidth.[2,4] The materials containing R^{3+} cations smaller than La^{3+} present a rather rich phenomenology associated with the MI transition. The gradual tilt of the NiO_6 octahedra as the R^{3+} size decreases governs the $3d$-$2p$ orbital overlap and determines the MI transition temperature (T_{MI}). Lacorre *et al.*[5] established the low-temperature insulator behavior of the Ni perovskites with R=Pr, Nd,…, Eu. They present orthorhombic symmetry (space group *Pbnm*) both above and below the MI transition. The subtle structural changes accompanying the metal-insulator transition, described in Ref. 6, do not imply a symmetry change. The insulating phase becomes magnetically ordered below T_N and the corresponding phase diagram as a function of the tolerance factor was mapped out.[7,8] The magnetic ordering of Ni below T_N (Refs. 9–11) is defined by an unexpected propagation vector $\mathbf{k}=(\frac{1}{2},0,\frac{1}{2})$, which implies that ferromagnetic (FM) and antiferromagnetic (AFM) Ni-O-Ni couplings alternate along the three pseudocubic axes. Based on these findings a nonuniform distribution of the confined e_g electron was predicted.[9–11] In these perovskites, Ni is in its low-spin Ni^{III} state ($t2_g^6e_g^1$) (Ref. 9) and, therefore, the σ^* band is twofold degenerated. However, the search for a structural modulation concomitant to the observed magnetic periodicities did not reveal the expected $2axbx2c$ superstructure reflections.[10,12] In order to explain the magnetic structure, Goodenough suggested that FM coupling might be a consequence of the covalent exchange[13] due to strong Ni-O hybridization, in contrast with the superexchange coupling responsible for the AFM interaction.

In spite of the electronic Jahn-Teller (JT) configuration of the low-spin Ni^{III} ion in the octahedral site, NiO_6 octahedra are almost regular in the first members of the RNiO$_3$ family,[7] indicating the absence of a cooperative JT deformation. This behavior contrasts with that shown by $LaMnO_3$ [containing

TABLE I. MI transition temperatures (K) for RNiO$_3$, obtained from DSC data in the heating and cooling runs.

R	Heating	Cooling
Ho	573	568
Y	582	579
Er	584	582
Lu	599	594

Mn^{3+}, a JT ion $(t2_g^3e_g^1)$], probably as a manifestation of the higher covalent character of Ni-O bonds. In addition, the signature of a significant electron-lattice coupling was observed in isotopically enriched RNiO$_3^{18}$ samples[14] and by infrared measurements.[15] These experiments demonstrate the importance of some oxygen vibrations in the MI transition, confirming that phonons participate in the electronic trapping. The electron-lattice coupling is expected to increase along the series, as R^{3+} cations become less electropositive.

Recently, we reported the occurrence of a charge disproportionation (CHD) of Ni^{3+} cations associated with the electronic localization in YNiO$_3$ (T_{MI}=582 K).[16] In the delocalized carriers regime, above T_{MI}, the structure is orthorhombic (*Pbnm*), similar to that of RNiO$_3$, R=Pr, Nd.[6,7] Below T_{MI} the symmetry changes to monoclinic (space group $P2_1/n$). The monoclinic symmetry in the localized carriers regime is due to the existence of two types of alternating NiO$_6$ octahedra. They can be ascribed to two different charge states on Ni or Ni-O bond states. We have shown that the symmetry for the smallest R^{3+} cations (R =Ho, Y, Er, Tm, Yb, and Lu) is also monoclinic at RT.[17] The comparative analysis of the structure of these insulators at RT demonstrated that, although the monoclinic distortion progressively increases as the R size diminishes, the amplitude of the charge modulation does not significantly evolve from Ho to Lu.[17]

In this work we have used high-resolution neutron (NPD) and synchrotron x-ray powder-diffraction techniques to analyze the metal-insulator transition in RNiO$_3$ oxides with R =Ho, Y, Er, and Lu, previously identified by differential scanning calorimetry (DSC) techniques. We present a detailed study of the structural changes associated with the electronic localization in these distorted perovskites.

II. EXPERIMENT

RNiO$_3$ (R=Y, Ho, Er, Lu) perovskites were prepared as polycrystalline powders by high-pressure solid-state reactions, as described elsewhere.[18] All the samples were single phase by diffraction measurements. DSC measurements were performed in a Mettler TA3000 system equipped with a DSC30 unit, in the temperature range from 300–863 K. The heating and cooling rates were 10 °C min^{-1}, using about 70 mg of the sample in each run. NPD measurements were carried out at the DB high-resolution diffractometer at Institut Laue Langevin (ILL)-Grenoble for R=Ho, Y, Er, and Lu. Samples were placed in a thin-walled vanadium can, inside a vanadium furnace working at 10^{-5} mPa. NPD data were always collected in a warming process. In order to avoid hysteresis-related effects the temperature was slowly increased (maximum 5 °C min^{-1}) and the sample was kept at the target temperature for 30 min before each data collection. In spite of the relatively small amount of sample available (500–800 mg), good quality patterns were obtained in the high-flux mode. The wavelength was 1.594 Å. Synchrotron x-ray-diffraction (SXRD) patterns for R=Ho and Y were collected on the BM16 diffractometer at the European Synchrotron Radiation Facility (ESRF), Grenoble. The samples were loaded in a borosilicate glass capillary ($\varnothing$=0.5 nm) and rotated during data collection. A short wavelength, λ =0.518 056(3) Å, was selected to reduce the absorption and to get the highest instrumental intensity and resolution. The working temperature was set with a hot air stream and controlled with a thermocouple very close to the capillary. Each SXRD run took about 3 h to have good statistics over the angular range 6°–43° in 2θ. All the powder patterns were analyzed by the Rietveld method, using the GSAS (SXRD) (Ref. 19) and FULLPROF (NPD) (Ref. 20) refinement programs. As the collecting temperatures for NPD and SXRD were not the same, combined refinements were only performed at RT for R=Ho and Y oxides. For the remaining

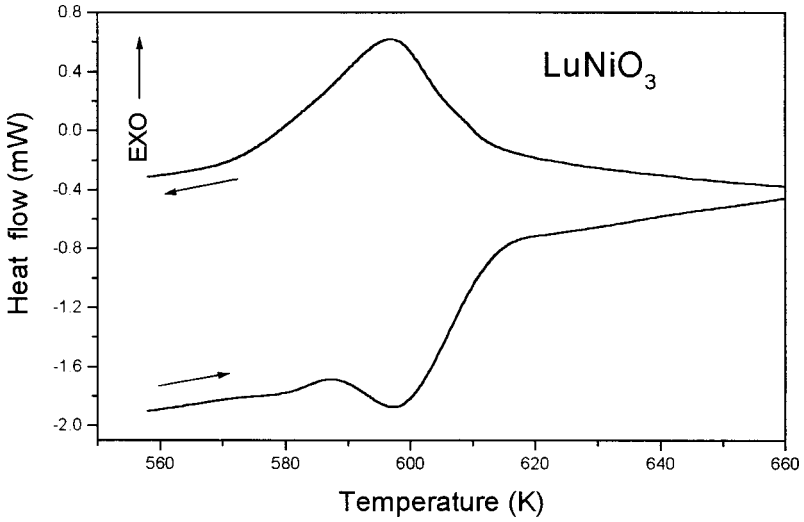

FIG. 1. DSC curves for LuNiO$_3$ obtained on the heating and cooling runs.

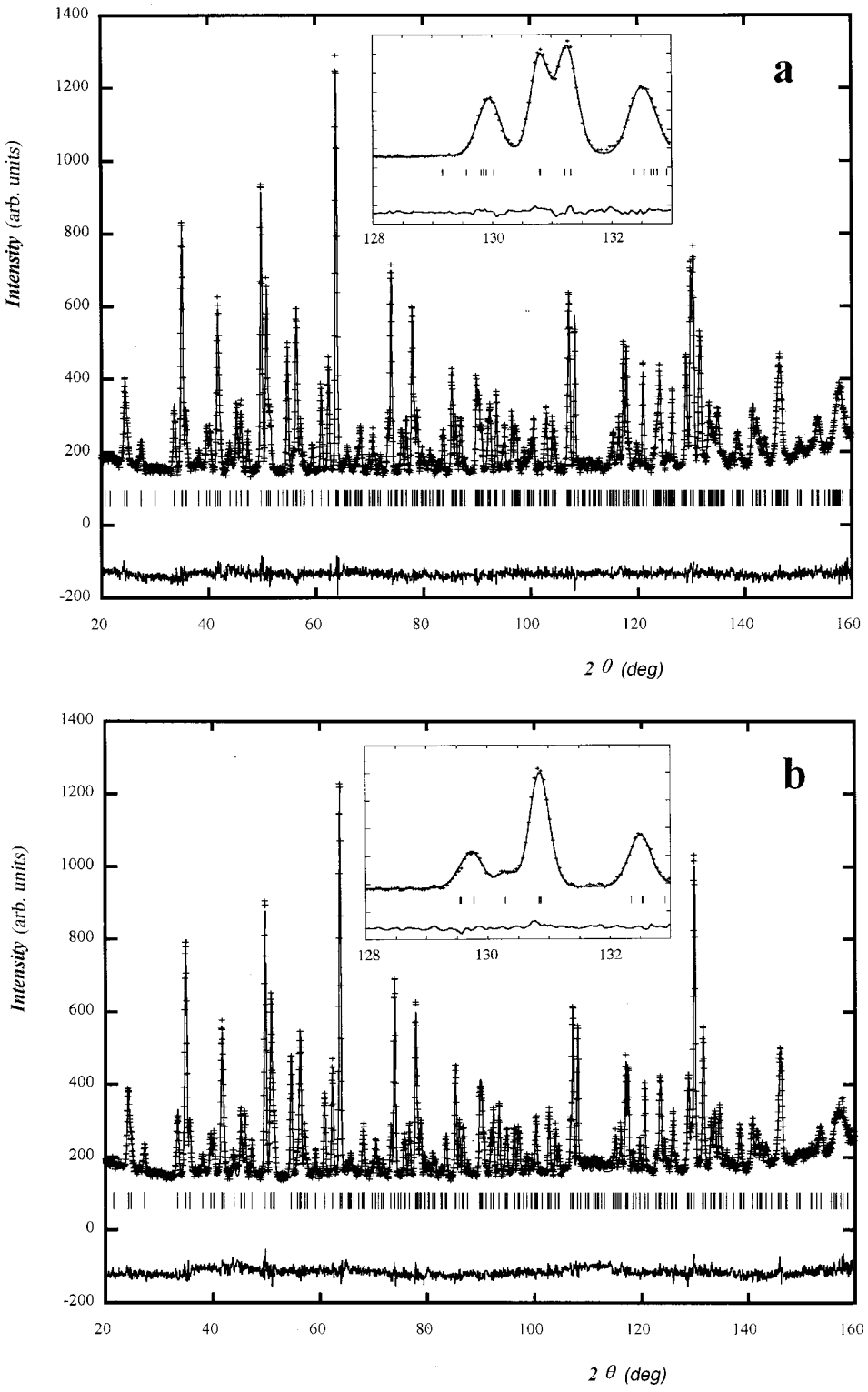

FIG. 2. Observed (crosses), calculated (full line), and difference (bottom) NPD Rietveld profiles for $YNiO_3$ (a) below T_{MI} (monoclinic) and (b) above T_{MI} (orthorhombic). The insets show enlarged high-angle 2θ regions where the effect of the structural rearrangement can be appreciated.

temperatures, SXRD data were used to follow the thermal unit-cell parameter evolution; the Ni-O bond distances were determined from NPD data given the higher accuracy of the refined oxygen positions.

III. DSC, NEUTRON, AND SYNCHROTRON RESULTS

The MI transition temperatures of $RNiO_3$, obtained from DSC measurements, are listed in Table I. Figure 1 illustrates the DSC curves for the last member of the series, $LuNiO_3$, obtained during the heating and cooling runs. The heating process exhibits a sharp endothermic peak centered at 599 K. The reverse transition, showing an exothermic peak, is observed during the cooling run. By analogy with the DSC peaks observed at the MI transition of the precedent members of the $RNiO_3$ family,[14,16] the peaks shown in Fig. 1 can be assigned to the corresponding MI transition in the $LuNiO_3$

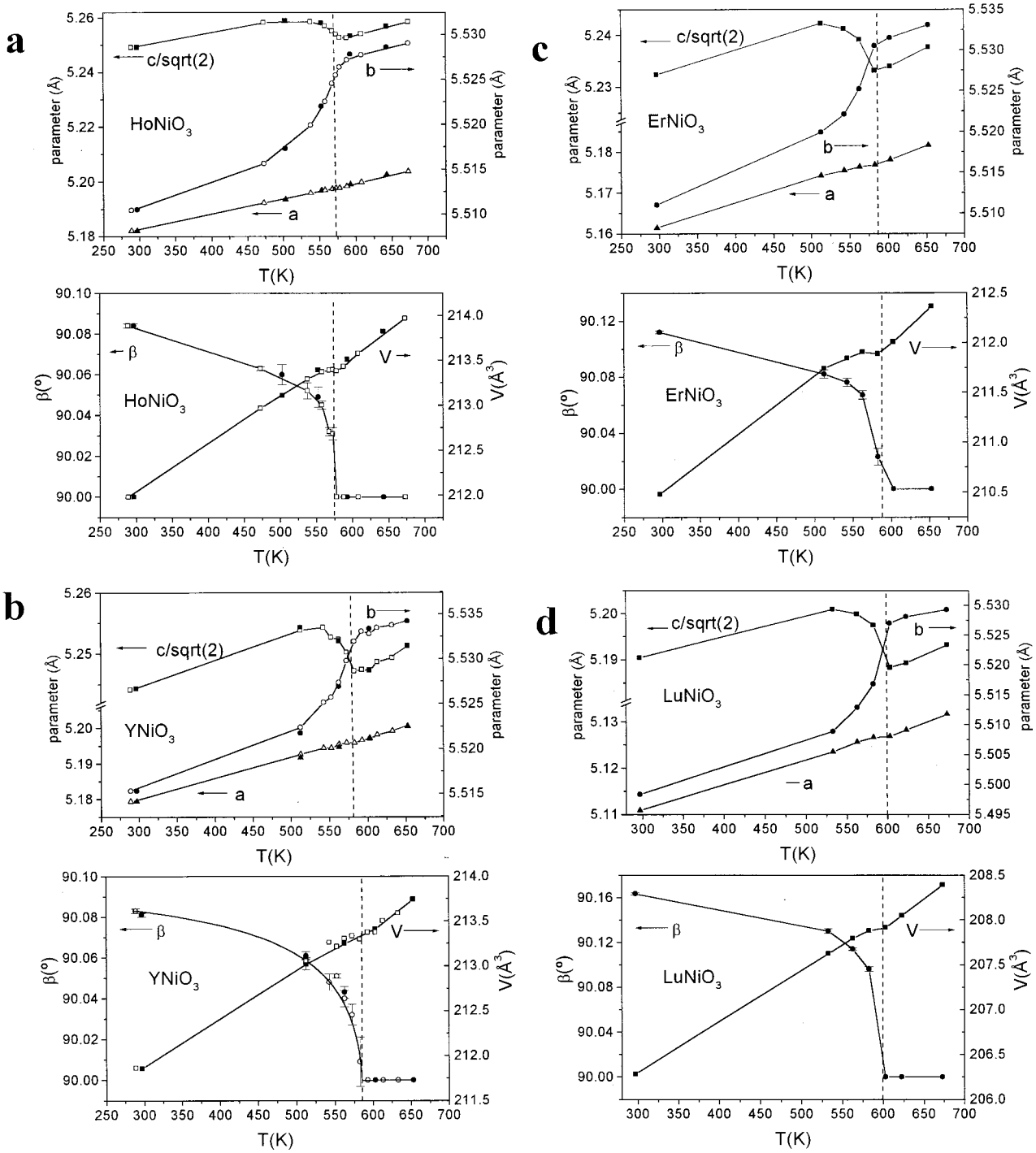

FIG. 3. Thermal variation of the unit-cell parameters of (a) $HoNiO_3$ [$T_{MI}=573$ K], (b) $YNiO_3$ [$T_{MI}=582$ K], (c) $ErNiO_3$ [$T_{MI}=584$ K], and (d) $LuNiO_3$ [$T_{MI}=599$ K] across the electronic delocalization. Open and full symbols correspond to SXRD and NPD data, respectively.

perovskite. The thermal hysteresis observed by DSC suggests that the transition is also first order for these strongly distorted perovskites. The heat transfer accounts for the entropy and lattice energy gain due to the electronic delocalization. Similar DSC curves were obtained for the remaining nickelates.

The structural refinements of the NPD and SXRD patterns collected below T_{MI} were performed in the monoclinic $P2_1/n$ space group, with unit-cell parameters related to a_0 (ideal cubic perovskite; $a_0 \approx 3.8$ Å) as $a \approx \sqrt{2}a_0$, $b \approx \sqrt{2}a_0$, $c \approx 2a_0$. The previously reported RT structures for $RNiO_3$ (R=Ho, Y, Er, and Lu)[17] were used as starting models. In the $P2_1/n$ phase there are two crystallographically independent Ni positions (Ni1 and Ni2), as well as three kinds of nonequivalent oxygen atoms (O1, O2, and O3) all in general positions. $Ni1O_6$ and $Ni2O_6$ octahedra alternate along the

three directions of the structure, in such a way that each $Ni1O_6$ octahedron is linked to six $Ni2O_6$ octahedra and vice versa. Table II contains the structural parameters from the refinements in the insulating region, 60–70 K below the respective transition temperature. The β parameter, characterizing the low-temperature monoclinic distortion, is in all cases smaller than 90.2°. Such a small deviation from 90° indicates a strongly pseudo-orthorhombic metric, which enforces the use of very high-resolution tools.

Above the transition temperature, the diffraction patterns were refined in the conventional orthorhombic *Pbnm* space group, with a single position for Ni atoms and two independent positions for oxygens, O1 ($4c$) and O2 ($8d$). Table III contains the atomic coordinates and other refined parameters for the four perovskites in the metallic regime, at temperatures 60–80 K above T_{MI}. As an example, Fig. 2 illustrates the good agreement between observed and calculated NPD profiles for the $YNiO_3$ perovskite at both sides of the transition. The insets illustrate enlarged regions at a high 2θ angle, showing important changes in the diffracted intensities as a consequence of the structural rearrangement across the transition.

The main component of the distortion from the ideal cubic perovskite structure corresponds to the tilt of the NiO_6 octahedra, of the type $a^-a^-c^+$ in the Glazer's nomenclature, in both the $P2_1/n$ and *Pbnm* space groups. Notice that in all cases $c/\sqrt{2}$ lies between *b* and *a*, which is the usual situation in perovskites where the primary distorting effect is steric. This distortion is due to the small size of the R^{3+} cations, which forces the NiO_6 octahedra to tilt in order to optimize the *R*-O distances.

IV. CHARGE DISPROPORTIONATION AND ITS TEMPERATURE DEPENDENCE

The analysis of the temperature-dependent diffraction data has allowed us to follow the structural changes concomitant with the electronic delocalization as the samples are heated through the transition. Figures 3(a)–3(c) show the thermal variation of the unit-cell parameters for $RNiO_3$ (R = Ho, Y, Er, Lu). The curves for the four oxides display the same pattern of behavior, with abrupt changes at the same temperatures where the DSC peaks were observed. The thermal evolution of the unit-cell parameters is very anisotropic. The largest changes correspond to the c ($\Delta c \approx -0.01$ Å) and b ($\Delta b \approx +0.008$ Å) parameters, whereas the change in the a parameter is comparatively much smaller ($\Delta a \approx -0.002$ Å). In the larger R perovskites, R = Pr, Nd, Sm,[6] the change in the a parameter is also the smallest. However, the changes in the b parameter are qualitatively different:it is interesting to note that the expansion of b across the transition shown in Fig. 3 for the insulating monoclinic $RNiO_3$ compounds (R = Ho, Y, Er, Lu) was not observed in the insulating orthorhombic perovskites (R = Pr, Nd, Sm), for which b contracts on heating across T_{MI}.[6]

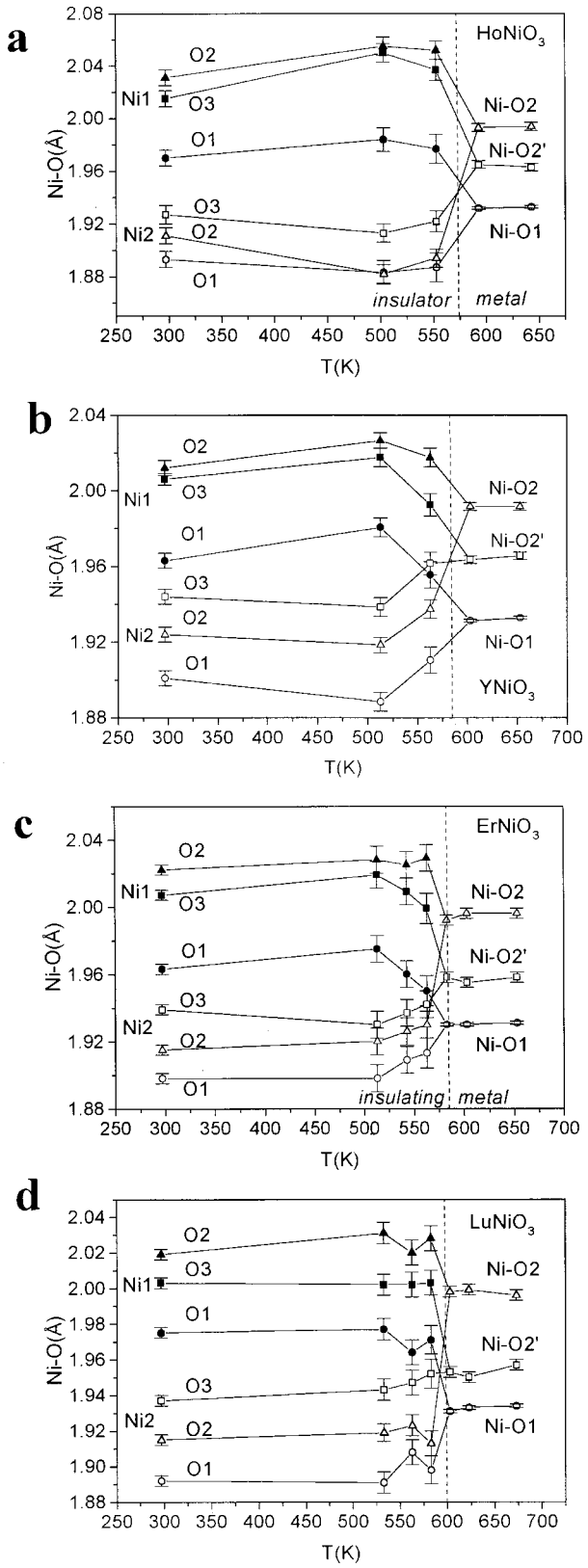

FIG. 4. Temperature dependence of individual Ni-O distances in (a) $HoNiO_3$, (b) $YNiO_3$, (c) $ErNiO_3$, and (d) $LuNiO_3$.

TABLE II. Positional and thermal parameters for RNiO$_3$ in the insulating regime, 60–70 K below the T_{MI} transition, refined in the monoclinic $P2_1/n$ space group, $Z=4$, from NPD data. Reliability factors for both patterns are also given.

R	Ho	Y	Er	Lu
T (K)	503	513	513	533
a (Å)	5.1935(1)	5.191 68(6)	5.1742(1)	5.1235(1)
b (Å)	5.5173(1)	5.521 74(6)	5.5199(1)	5.5089(1)
c (Å)	7.4372(2)	7.430 67(9)	7.4137(1)	7.3552(1)
β (°)	90.060(4)	90.061(2)	90.082(3)	90.130(2)
V (Å^3)	213.105(8)	213.015(6)	211.741(7)	207.623(6)
R 4e (x y z)				
x	0.9817(7)	0.9817(4)	0.9810(7)	0.9771(7)
y	0.0717(4)	0.0717(2)	0.0713(4)	0.0770(4)
z	0.2526(14)	0.2518(8)	0.2530(13)	0.2529(9)
B_{iso} (Å^2)	0.56(5)	0.60(2)	0.61(5)	0.52(5)
Ni1 2d ($\frac{1}{2}$ 0 0)				
B_{iso} (Å^2)	0.52(11)	0.65(6)	1.06(12)	0.45(7)
Ni2 2c ($\frac{1}{2}$ 0 $\frac{1}{2}$)				
B_{iso} (Å^2)	0.29(9)	0.32(6)	0.44(9)	0.40(7)
O1 4e (x y z)				
x	0.0969(8)	0.0990((0))	0.1031(8)	0.1100(7)
y	0.4684(7)	0.4695(4)	0.4693(7)	0.4626(6)
z	0.243(1)	0.2436(7)	0.2447(11)	0.2440(8)
B_{iso} (Å^2)	0.70(7)	0.54(4)	0.78(6)	0.70(6)
O2 4e (x y z)				
x	0.7046(13)	0.6981(9)	0.696(1)	0.6933(10)
y	0.313(1)	0.3099(9)	0.312(1)	0.3137(11)
z	0.047(1)	0.0467(6)	0.048(1)	0.0538(7)
B_{iso} (Å^2)	0.67(12)	0.47(7)	0.78(11)	0.72(8)
O3 4e (x y z)				
x	0.182(1)	0.1881(9)	0.187(1)	0.185(1)
y	0.208(1)	0.2057(8)	0.207(1)	0.2016(11)
z	0.945(1)	0.9460(7)	0.946(1)	0.9437(8)
B_{iso} (Å^2)	0.60(12)	0.82(8)	1.2(1)	0.92(8)
Reliability factors				
χ^2	2.25	1.70	1.73	1.50
R_p (%)	4.23	3.45	4.29	4.08
R_{wp} (%)	5.29	4.42	5.41	5.11
R_{exp} (%)	3.53	3.39	4.12	4.18
R_I (%)	14.6	5.90	11.1	9.36

Figures 3(a)–3(d) also illustrate the anomaly of the volume on heating across the transition, due to the disappearance of the CHD. We can define a superimposed ''contraction'' of the volume $\Delta V/V$ with respect to the extrapolated thermal expansion if no electronic effects were present at T_{MI}. For R=Ho, Y, Er, and Lu, $\Delta V/V$ is 0.07%, 0.03%, 0.12%, and 0.04%, respectively. This volume contraction is smaller than that observed in the first terms of the series: $\Delta V/V$ is 0.25%, 0.23%, and 0.15% for R=Pr, Nd, and Sm.[6] The temperature evolution of the β angle is also depicted in Figs. 3(a)–3(d). Although the deviation from 90° is small, the change to a monoclinic symmetry below T_{MI} is apparent in the four compounds. It should be noted that, upon cooling the sample well below T_{MI} the distortion evolves progressively: the β angle is still rising at 300 K.

The inhomogeneous charge distribution at T_{MI} is evidenced by a symmetry breaking of the oxygen positions. Therefore it is interesting to follow the evolution of the interatomic Ni-O bonds. The thermal dependence of Ni-O distances obtained from the analysis of the NPD data is displayed in Figs. 4(a)–4(d) for the four studied compounds. Essentially, the results indicate that the CHD completely

TABLE III. Positional and thermal parameters for $R\mathrm{NiO_3}$ in the metallic regime, 60–70 K above the T_{MI} transition, refined in the orthorhombic $Pbnm$, $Z=4$, from NPD data. Reliability factors are also given.

R	Ho	Y	Er	Lu
T (K)	643	653	653	673
a (Å)	5.2026(1)	5.200 51(7)	5.1816(1)	5.1316(1)
b (Å)	5.5286(1)	5.534 19(8)	5.5331(1)	5.5293(1)
c (Å)	7.4343(2)	7.4264(1)	7.4072(1)	7.3443(1)
V (Å^3)	213.823(8)	213.742(7)	212.363(7)	208.389(6)
R 4c $(x\ y\ \frac{1}{4})$				
x	0.9816(8)	0.9818(5)	0.9820(6)	0.9782(6)
y	0.0714(4)	0.0711(3)	0.0723(3)	0.0765(4)
B (Å^2)	0.71(5)	0.79(3)	0.88(4)	0.69(5)
Ni 4b $(\frac{1}{2}\ 0\ 0)$				
B (Å^2)	0.64(4)	0.73(2)	1.06(3)	0.65(3)
O1 4c $(x\ y\ \frac{1}{4})$				
x	0.0968(8)	0.0985(5)	0.1008(6)	0.1113(7)
y	0.4682(8)	0.4701(5)	0.4703(6)	0.4629(7)
B (Å^2)	0.88(7)	0.82(4)	1.14(5)	0.83(6)
O2 8d $(x\ y\ z)$				
x	0.6939(6)	0.6931(4)	0.6924(5)	0.6890(5)
y	0.3037(6)	0.3037(4)	0.3055(5)	0.3076(5)
z	0.0505(4)	0.0496(3)	0.0495(3)	0.0530(3)
B (Å^2)	1.05(5)	1.04(3)	1.44(4)	1.00(4)
Reliability factors				
χ^2	2.42	2.30	2.53	1.60
R_p (%)	4.47	4.11	3.39	4.23
R_{wp} (%)	5.59	5.16	4.25	5.32
R_{exp} (%)	3.59	3.40	2.67	4.20
R_I (%)	18.2	9.66	12.8	11.7

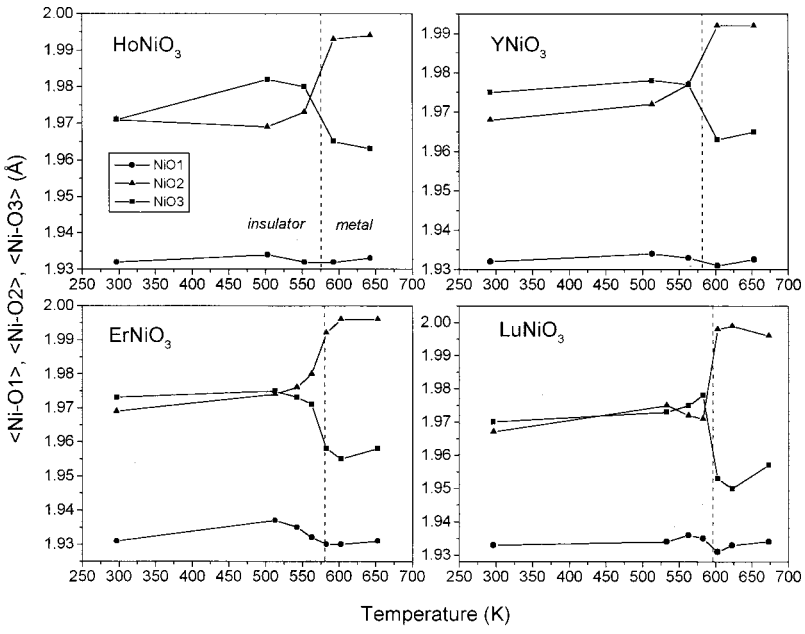

FIG. 5. Thermal evolution of the average ⟨Ni-O1⟩, ⟨Ni-O2⟩, and ⟨Ni-O3⟩ bond lengths for the four nickelates.

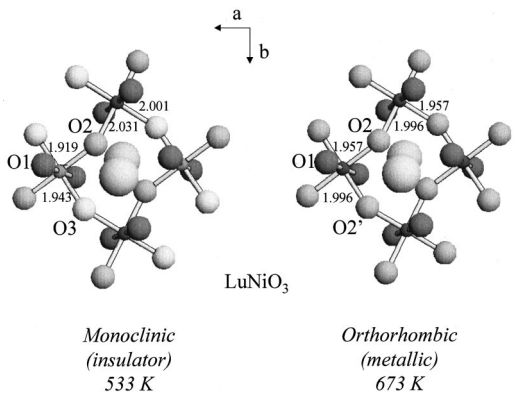

FIG. 6. Projection of the $LuNiO_3$ crystal structure along the *c*-axis direction, illustrating the bond-length changes induced by the electronic delocalization: (a) below T_{MI} (insulating) and (b) above T_{MI} (metallic).

vanishes at the MI transition in all of the samples. Data in Fig. 4 illustrate the abrupt convergence of the two sets (Ni1 and Ni2) of three Ni-O bond lengths, in the monoclinic-insulating phase, to three unique Ni-O distances in the orthorhombic-metallic phase. The two apical Ni1-O1 and Ni2-O1 bond lengths result in a single Ni-O1 distance in the orthorhombic phase, Ni1-O2 and Ni2-O2 bonds converge to Ni-O2, and Ni1-O3 and Ni2-O3 converge to Ni-O2, the last two bonds approximately lying in the *ab* plane. Namely, each symmetrically bonded pair Ni-O-Ni above T_{MI} splits into long and short Ni-O bonds. The result is an asymmetric distribution of the charges that implies different overlap integrals.

In the former members of the series (R=Pr, Nd) an isotropic contraction of Ni-O distances by 0.004 Å was observed at T_{MI}, coupled to a tilting of the NiO_6 octahedra by 0.5°.[6] This effect was triggered by the sudden electronic delocalization. For the present compounds, the changes in Ni-O bond distances exhibit interesting anisotropic features, mainly concerning O2 and O3 oxygens in the basal *ab* plane. Figure 5 shows the thermal evolution of the mean ⟨Ni-O1⟩, ⟨Ni-O2⟩, and ⟨Ni-O3⟩ bond distances, obtained by averaging the bond distances from Ni1 and Ni2 atoms to every oxygen. As observed for the four nickelates, there is an abnormal expansion of one of the bonds, ⟨Ni-O2⟩, while the ⟨Ni-O1⟩ and ⟨Ni-O3⟩ average distances decrease when entering the metallic state, as expected. This result would suggest the formation of an anisotropic metallic state and could imply an important degree of orbital polarization in the high-temperature orthorhombic phase.

The origin of the abrupt increase of the *b* unit-cell parameter when heating across the transition can be understood with the help of Fig. 6. This figure shows a projection of the monoclinic (at 533 K) and orthorhombic (at 673 K) structures on the basal *ab* plane for $LuNiO_3$. For the sake of clarity, only one layer of octahedra is represented. In the monoclinic phase we observe that, given the tilting scheme and the large magnitude of the octahedral tilts, Ni1-O2 (2.031 Å for $LuNiO_3$) and Ni2-O3 (1.943 Å for $LuNiO_3$) bonds form a small angle (≈25°) with the *b* axis, therefore the magnitude of these bond lengths mostly determine the size of this parameter. Above the transition, in the orthorhombic phase, both bond lengths become equivalent and take a value of 1.996 Å. This is the longest distance in the NiO_6 octahedra of the orthorhombic phase and, therefore, the expansion of the *b* axis is determined by this particular re-

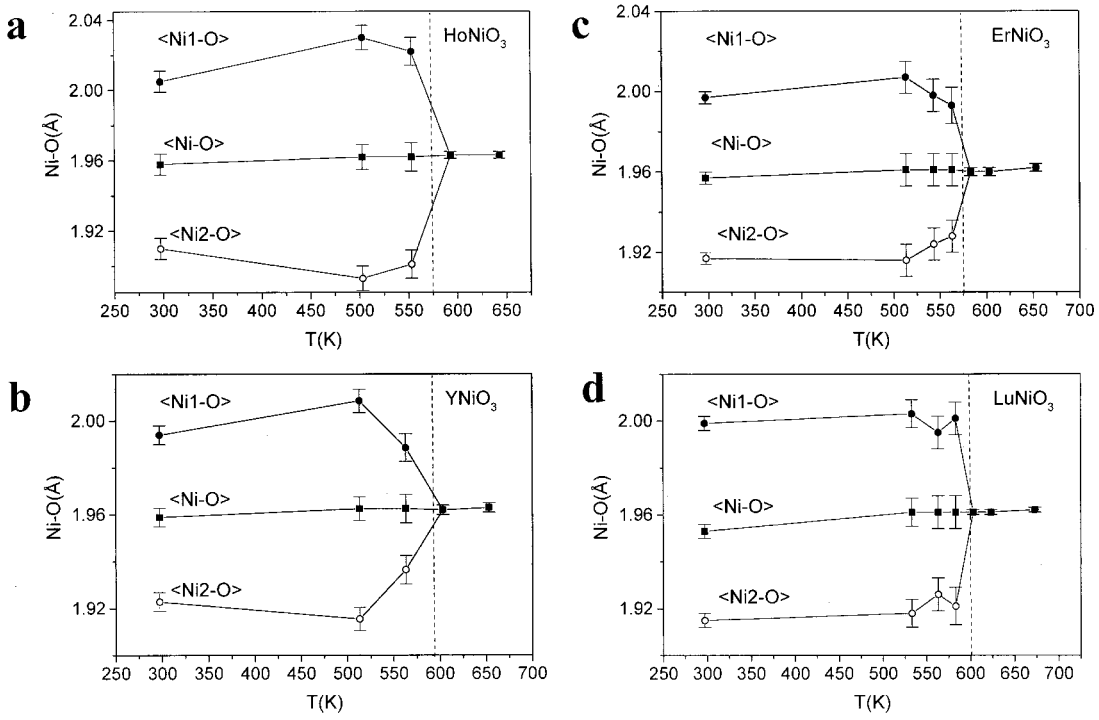

FIG. 7. Thermal evolution of the average ⟨Ni1-O⟩, ⟨Ni2-O⟩, and ⟨Ni-O⟩ bond lengths of the NiO_6 octahedra for (a) $HoNiO_3$, (b) $YNiO_3$, (c) $ErNiO_3$, and (d) $LuNiO_3$.

TABLE IV. Distortion parameter Δ_d ($\times 10^4$) for NiO_6 octahedra with an average Ni-O distance $\langle d \rangle$, defined as $\Delta_d = (1/6)\Sigma_{n=1,6}\ [(d_n - \langle d \rangle)/\langle d \rangle]^2$. Above the MI transition, the values for the unique NiO_6 octahedra are included under the heading Δ_d(Ni1O6).

R = Ho			R = Y		
T (K)	Δ_d(Ni1O6)	Δ_d(Ni2O6)	T (K)	Δ_d(Ni1O6)	Δ_d(Ni2O6)
297	1.66	0.53	297	1.20	0.83
503	2.54	0.58	513	0.98	1.15
553	2.57	0.63	563	1.64	1.16
593	1.61		603	1.61	
643	1.61		653	1.53	
R = Er			R = Lu		
297	1.57	0.77	297	0.83	0.92
513	1.33	0.49	533	1.21	1.23
543	1.92	0.36	563	1.37	0.70
563	2.67	0.38	583	1.37	1.40
583	1.67		603	2.02	
603	1.93		623	2.04	
653	1.85		673	1.70	

distribution of bond lengths. A contraction of the cell parameters is usually expected in an isotropic transition-metal oxide when entering the metallic state (in the absence of Jahn-Teller distortions or the stabilization of a particular orbital configuration). We thus conclude that, in these small rare-earth nickelates, the expansion of the *b* parameter seems to be a signature of the presence of the CHD that vanishes at T_{MI}.

To characterize the thermal dependence of the amplitude of the CHD, it is necessary to study the temperature variation of the average Ni1-O and Ni2-O distances, shown in Figs. 7(a)–7(c). These plots suggest a gradual increase of the degree of charge disproportionation (i.e., the difference between the average size of $Ni1O_6$ and $Ni2O_6$ octahedra) on increasing temperature in the insulating regime, to reach a maximum of 60–80 K below the MI transition. This effect is more significant for $YNiO_3$ and $HoNiO_3$ and becomes almost unnoticeable in $LuNiO_3$, in which the maximum difference in size between large (Ni1) and small (Ni2) octahedra is already established at RT. This observation could be related to the higher electron-lattice coupling expected for the more distorted Lu compound. A more complete study of the evolution of the degree of charge disproportionation below RT would be necessary before drawing further conclusions.

Finally, it is interesting to examine the evolution of the distortion of the NiO_6 octahedra across the transition, defining the distortion parameter $\Delta_d = (1/6)\Sigma_{n=1,6}[(d_n - \langle d \rangle)/\langle d \rangle]^2$ (Table IV). At room temperature, the distortion parameters fall within the interval $0.8-1.7\times 10^{-4}$. Notice that in the four compounds this static distortion is one order of magnitude bigger than in the insulating phase with R = Sm ($\Delta_d \approx 1.6\times 10^{-5}$) (Ref. 12) and two orders bigger than for R = Pr ($\Delta_d \approx 1.4\times 10^{-6}$).[6] This is indicative of a systematic increase of the deformation going to smaller rare-earth cations. On the other hand the deformation is very small compared to the expected value for a JT distorted octahedra. In particular, it is around 30 times smaller than the deformation found in $LaMnO_3$ ($\Delta_d \approx 3.3\times 10^{-3}$).[12] But, most interestingly, Δ_d increases with temperature and reaches its maximum value at temperatures close to T_{MI}. In particular, values of Δ_d as high as 2.57×10^{-4} (R = Ho) or 2.67×10^{-4} (R = Er) are observed immediately before the transition. This is coherent with the strong anisotropical changes that take place in the Ni-O bond distances concomitant with the electronic delocalization, which seems to be characteristic of the small rare-earth nickelates.

V. CONCLUSIONS

DSC measurements were used to determine the metal-insulator transition temperature of highly distorted $RNiO_3$ perovskites (R = Ho, Y, Er, and Lu), prepared under high-oxygen pressure. The transitions occur well above RT, between 573 and 600 K. Based on high- resolution neutron- and synchrotron diffraction data, we have reported the evolution of the unit-cell parameters and crystal structure between 300 and 700 K. The changes in Ni-O distances on heating were described in detail, showing that the CHD (defined by the size difference between large and small NiO_6 octahedra) progressively increases to a maximum value, about 60–80 K below T_{MI}, and then suddenly vanishes at T_{MI} in the four compounds. An unexpected expansion of the *b* unit-cell parameter is observed across the transition, opposite to the sudden contraction experienced by *a* and *c* parameters. This is the result of an extremely anisotropic rearrangement of Ni-O bond distances in the basal *ab* plane, not observed in the former members of the $RNiO_3$ series (R = Pr, Nd, Sm$\cdots$). Further work is necessary to give a complete electronic picture of the origin of the observed anisotropy.

ACKNOWLEDGMENTS

The authors would like to thank Dr. Eric Dooryhee for assistance during data collection on BM16 and The ESRF and ILL for making available the beam time. Financial support is acknowledged from the CE (OXSEN-TMR) and OCYT-CYCyT (MAT97-0699, PB97-1181, and PB97-1175 projects).

*Corresponding author. Email address: ja.alonso@icmm.csic.es

[1] J. B. Goodenough and P. M. Raccah, J. Appl. Phys. **36**, 1031 (1965).
[2] J. B. Goodenough, N. F. Mott, M. Pouchard, G. Demazeau, and P. Hagenmuller, Mater. Res. Bull. **8**, 647 (1973).
[3] J.-S. Zhou, J. B. Goodenough, B. Dabrowski, P. W. Klamut, and Z. Bukowski, Phys. Rev. Lett. **84**, 526 (2000).
[4] K. Sreedhar *et al.*, Phys. Rev. B **46**, 6382 (1992).
[5] P. Lacorre, J. B. Torrance, J. Pannetier, A. I. Nazzal, P. W. Wang, and T. C. Huang, J. Solid State Chem. **91**, 225 (1991).
[6] J. L. García-Muñoz, J. Rodríguez-Carvajal, P. Lacorre, and J. B. Torrance, Phys. Rev. B **46**, 4414 (1992).
[7] J. B. Torrance, P. Lacorre, A. I. Nazzal, E. J. Ansaldo, and Ch. Niedermayer, Phys. Rev. B **45**, 8209 (1992).
[8] J. A. Alonso, M. J. Martínez-Lope, M. T. Casais, J. L. Martínez, G. Demazeau, A. Largeteau, J. L. García-Muñoz, A. Muñoz, and M. T. Fernández-Díaz, Chem. Mater. **11**, 2463 (1999).
[9] J. L. García-Muñoz, J. Rodríguez-Carvajal, and P. Lacorre, Europhys. Lett. **20**, 241 (1992).
[10] J. L. García-Muñoz, J. Rodríguez-Carvajal, and P. Lacorre, Phys. Rev. B **50**, 978 (1994).
[11] J. L. García-Muñoz, P. Lacorre, and R. Cywinski, Phys. Rev. B **51**, 15 197 (1995).
[12] J. Rodríguez-Carvajal, S. Rosenkranz, M. Medarde, P. Lacorre, M. T. Fernández-Díaz, F. Fauth, and V. Trounov, Phys. Rev. B **57**, 456 (1998).
[13] J. B. Goodenough, J. Solid State Chem. **127**, 126 (1996).
[14] M. Medarde, P. Lacorre, K. Conder, F. Fauth, and A. Furrer, Phys. Rev. Lett. **80**, 2397 (1998).
[15] N. E. Massa, J. A. Alonso, and M. J. Martínez-Lope, Phys. Rev. B **56**, 986 (1997).
[16] J. A. Alonso, J. L. García-Muñoz, M. T. Fernández-Díaz, M. A. G. Aranda, M. J. Martínez-Lope, and M. T. Casais, Phys. Rev. Lett. **82**, 3871 (1999).
[17] J. A. Alonso, M. J. Martínez-Lope, M. T. Casais, J. L. García-Muñoz, and M. T. Fernández-Díaz, Phys. Rev. B **61**, 1756 (2000).
[18] J. A. Alonso, M. J. Martínez-Lope, M. T. Casais, M. A. G. Aranda, and M. T. Fernández-Díaz, J. Am. Chem. Soc. **121**, 4754 (1999).
[19] A. C. Larson and R. B. von Dreele, Los Alamos National Laboratory Report No. LA-UR-86-748, 1994 (unpublished).
[20] J. Rodríguez-Carvajal, Physica B **192**, 55 (1993).